Mechanism of Wear and Ripple Formation Induced by the Mechanical Action of an Atomic Force Microscope Tip

Aleksander E. Filippov,[1] Valentin L. Popov,[2] and Michael Urbakh[3]

[1]*Donetsk Institute for Physics and Engineering of NASU, 83144, Donetsk, Ukraine*
[2]*Technische Universität Berlin, Straße des 17. Juni 135, D - 10623 Berlin, Germany*
[3]*School of Chemistry, Tel Aviv University, 69978 Tel Aviv, Israel*

(Received 25 August 2010; published 14 January 2011)

We propose a model for a description of formation of quasiperiodic nanoscale patterns induced by scratching a surface with an atomic force microscope tip. The simulations demonstrate that the interplay between the developing surface corrugation and the frictional stress produced by the moving tip plays a decisive role in the formation of the regular ripples. Our model reveals the size and shape of the tip as the main factors that determine periodicity and amplitudes of the patterns, and it allows experimental observations to be explained. It is shown that the wear at the nanoscale cannot be explained by conventional macroscopic wear theories.

DOI: 10.1103/PhysRevLett.106.025502 PACS numbers: 62.20.Qp, 81.16.Rf, 81.40.Pq

The practical importance and relevance to basic scientific questions have motivated recent studies towards understanding mechanisms of wear at the nanoscale [1–9]. The atomic force microscope (AFM) is ideally suited to gain insight into the problem, as it allows us to perform localized and controllable modifications of surface structure and *in situ* imaging of the resulting topography with nanometer scale resolution. An AFM tip moving over the surface induces the rupture of chemical bonds and displacement of atoms or small clusters, therefore producing a change in surface topography. It has been reported that repeated scratching of surfaces of different materials, such as polymers [10], ionic crystals, metals [2,11], and semiconductors [12] resulted in the formation of quasiperiodic nanoscale patterns (ripples). Similar structures also can be created by ion beam sputtering [13], and they are commonly observed on macroscopic scales. In spite of the universal nature of the process of pattern formation and the growing efforts in investigations of this phenomenon [2,7,10–14], many fundamental aspects of ripple formation induced by a localized moving perturbation are still not understood.

In this Letter we propose a model for a description of formation of regular ripples induced by scratching a surface with an AFM tip that is repeatedly scanned along a line. The simulations demonstrate that interplay between the developing surface corrugation and the lateral stress produced by the moving tip plays a decisive role in the formation of the quasiperiodic nanoscale patterns. Our model reveals the main factors that determine periodicity and amplitudes of the patterns, and it allows experimental observations to be explained [2,11,12].

A schematic representation of the model is shown in Fig. 1. A tip is elastically coupled to a support with a spring having an effective spring constant k and experiences a constant loading force F_N in z direction while it is pulled over the surface with a constant velocity V along the x direction. Three-dimensional frictional motion of the driven tip can be modeled by the following Langevin equations:

$$M\ddot{x} + \eta\dot{x} - F_x^{(\mathrm{int})} + k(x - Vt) = f_x, \tag{1}$$

$$M\ddot{y} + \eta\dot{y} - F_y^{(\mathrm{int})} + k(y - y_0) = f_y, \tag{2}$$

$$M\ddot{z} + \eta\dot{z} - F_z^{(\mathrm{int})} - F_N = f_z. \tag{3}$$

Here (x, y, z) and M are the position and effective mass of the tip, η is the damping constant (the same for x, y, and z directions). The effect of thermal fluctuations on the tip motion is given by the random forces $f_{x,y,z}$ which are δ correlated, $\langle f_s(t) f_{s'}(t')\rangle = 2\eta k_B T \delta_{ss'}\delta(t - t')$, $s = x$, y, z, and $F_{x,y,z}^{(\mathrm{int})}$ are the interaction forces between the tip and the underlying substrate.

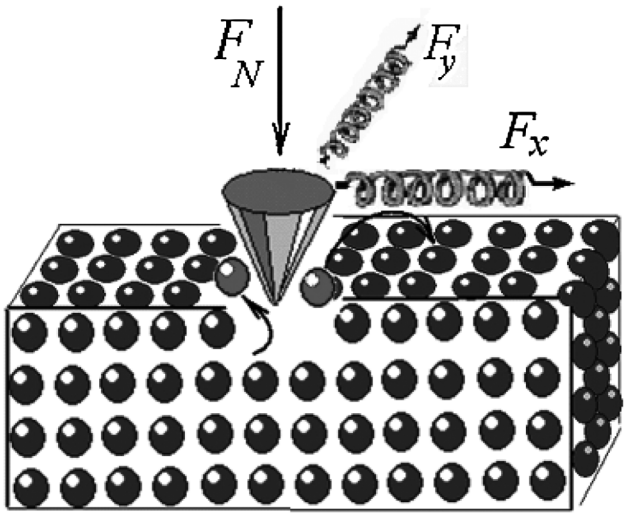

FIG. 1. Schematic sketch of the model setup.

The tip-surface interactions in the lateral x, y directions are approximated by a sum of repulsive Gaussian potentials

$$F^{(\mathrm{int})}_{x(y)}(x,y,z) = -U_0 \frac{\partial}{\partial x(y)} \sum_{i,j,k} \exp\{-[(x-x_i)^2 + (y - y_j)^2 + (z-z_k)^2]/r_0^2\}, \quad (4)$$

which are spatially centered at the positions of surface atoms (x_i, y_j, z_k), occupying sites of a cubic lattice, which are marked by $i, j, k = 0, \pm 1, \pm 2, \ldots$. In order to accelerate the numerical simulations only atoms with a distance smaller than $5r_0$ from the tip were included in the sum. The parameter r_0 defines a characteristic range of the tip-surface interaction and depends on the radius of the tip apex. In the normal direction we assumed an exponential decrease of the tip-surface repulsion with a distance from the surface atoms,

$$F^{(\mathrm{int})}_{z} = -U_z \frac{\partial}{\partial z} \sum_{k} \exp[-(z-z_k)/r_0], \quad (5)$$

where, as above, the sum includes all atoms with a distance smaller than $5r_0$ from the tip.

In this Letter we focus on the mechanical action of the scanning tip that leads to the removal, displacement, and rearrangement of surface atoms. Recent scanning probe microscopy experiments [6,7,15] demonstrated that such a wear process occurs through an atom-by-atom detachment, which in turn implies the breaking of individual bonds. The bond breaking can be considered as a thermally activated process governed by the Arrhenius type kinetics with an activation barrier that decreases with an increase of the friction stress [16,17]. Here, we neglect the effect of thermal fluctuations on the atom detachment and assume that the tip is able to remove a surface atom when the absolute value of the instantaneous force acting on the atom $|F_{\text{tip-atom}}|$ exceeds a threshold value F_{th}. Including the Arrhenius kinetics of bond rupture does not change the conclusions of this work.

Rather than using a dynamic description of motion of detached atoms, we utilize a procedure that defines the displacement of the atoms located in the uppermost layer. At each time-step (n) of the simulations, we examine the detachment condition $|F_{\text{tip-atom}}| > F_{\text{th}}$. If it is fulfilled, the corresponding atom is removed from its position at the previous time step, $(n-1)$, and located in a new one: $\{x_i^{n-1}, y_j^{n-1}, z_k^{n-1}\} \rightarrow \{x_{i'}^{n}, y_{j'}^{n}, z_{k'}^{n}\}$. We assume that the displacement in the $\{x, y\}$ plane occurs at the angle φ with respect to the pulling direction x, and it is proportional to the force acting on the atom at the moment of detachment. The impact angle φ is determined by the shape of the tip. We discuss a dependence of the results on the value of φ below. Thus, the new $\{x, y\}$ coordinates of the atom are given by the following equations:

$$x_{i'}^{n} = x_i^{n-1} + a \| \cos\varphi |F_{\text{tip-atom}}|/F_0 \|, \quad (6)$$

$$y_{j'}^{n} = y_j^{n-1} \pm a \| \sin\varphi |F_{\text{tip-atom}}|/F_0 \|, \quad (7)$$

where F_0 is a normalization constant and the symbol $\|\|$ denotes the closest integer number to the argument, since the atoms occupy sites of the discrete lattice. The sign of the displacement in the y direction [see Eq. (7)] has been chosen randomly taking into account that atoms can be displaced both to the right and to the left of the driving direction x with equal probability.

Upon receiving new lateral coordinates $\{x_{i'}^{n}, y_{j'}^{n}\}$, the removed atom also obtains a new z coordinate that corresponds to a position on top of the surface atom with the coordinates $\{x_{i'}^{n}, y_{j'}^{n}\}$. Thus, the removed atoms assemble a new surface layer. It should be noted that the described procedure may lead to a highly jagged surface with sudden changes in heights (z coordinates) of the adjacent surface atoms. In order to mimic the effect of surface diffusion that smooths out the height gradients, we exclude configurations for which differences in heights of any adjacent surface atoms exceed the lattice spacing a. This has been done in the following way: we calculated the differences between the heights of the displaced atom and its neighbors, $\Delta z = z_{k'}^{n} - z_{k''}^{n-1}$, and if at least one of them exceeded a ($\Delta z > a$), the atom was shifted by the lattice spacing in the direction of the steepest slope. For cases in which $\Delta z > a$ for more than one of the neighboring atoms, the direction of atom displacement was chosen randomly from among the directions with steep slopes.

For a wide range of parameters, our model exhibits a formation of quasiperiodic surface patterns while scratching the surface with the AFM tip (see Figs. 2 and 3), as it was observed in experiments [2,10–12]. Figure 2(a) shows the topography of a groove calculated after scratching the surface 100 times along a line with a normal load $F_N = 25$ nN, scanning velocity $V = 2\mu$m/s, and impact angle $\varphi = \pi/4$. In simulations we start with the atomically flat surface and analyze time evolution of lateral forces and topography while scratching the surface. Initial stages of scratching involve a displacement of a very limited number of atoms, and in this case, the lateral force is low and no structure can be recognized. Afterwards, the tip motion slows down at the slopes of randomly produced mounds, the lateral stress is built up, and as a result, additional atoms detach from the surface in front of the mound and are transferred to it. When the lateral force acting on the tip becomes high enough to pull it over the mound, the tip movement accelerates, its interaction with the substrate is reduced, and the detachment of atoms diminishes. During the subsequent scans the existing mounds collect additional atoms and grow, while the pits between them get deeper. Thus, the tip motion can be represented as a set of alternating segments of accelerated and decelerated stages which correspond to the regions of reduced and enhanced wear, respectively. In accordance with experimental observations [11], we found that the surface corrugation along the scan line is

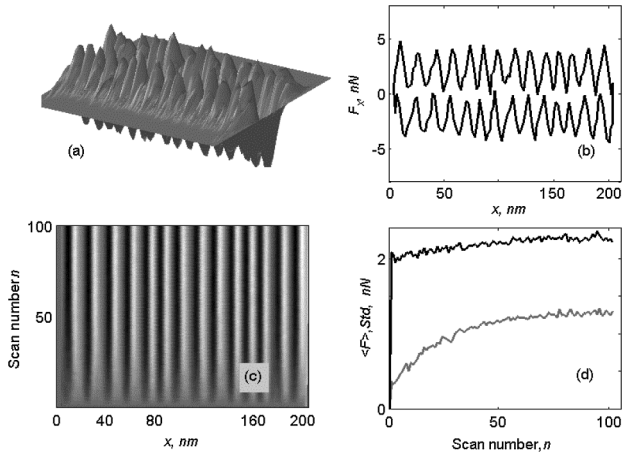

FIG. 2. (a) and (b) Topography of the groove and the lateral force loop calculated after 100 scans. The upper and lower branches of the force have been obtained by scanning forward and backward, respectively. (c) Development of the lateral force with the number of scans, n, during forward and backward scratching over a line of 200 nm length. Darker colors correspond to a stronger force. (d) Variation of the mean lateral force (black curve) and its standard deviation (gray curve) while producing the quasiperiodic pattern. Parameter values used in simulations: $k = 2$ N/m, $M = 2 \times 10^{-11}$ kg, $V = 2 \times 10^3$ nm/s, $a = 0.4$ nm, $r_0 = 3$ nm, $F_N = 25$ nN, $\eta = 10^{-5}$ kg/s, $U_0 = 1.1$ eV, $U_z = 0.75$ eV, $k_BT = 0.025$ eV, $F_{\text{th}} = 10^{-2}$ nN, $F_0 = 0.5F_{\text{th}}$, $\varphi = \pi/4$. The numbers of lattice cells along the x, y directions are $N_x = 512$; $N_y = 40$.

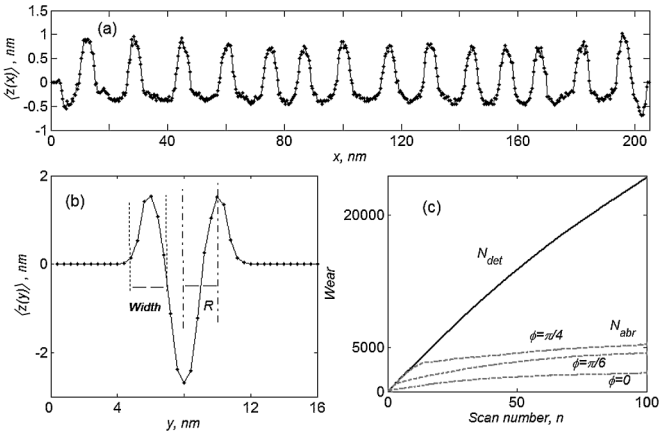

FIG. 3. Surface corrugations, $\langle z(x)\rangle$ and $\langle z(y)\rangle$, along (a) and across (b) the groove after scratching the surface 100 times. (c) Solid and dashed curves, respectively, show how the number of removed atoms $N_{\text{det}}(n)$ and the surface abrasion $N_{\text{abr}}(n)$ change with respect to the number of scans. Calculations show a strong effect of the impact angle φ on $N_{\text{abr}}(n)$, while $N_{\text{det}}(n)$ is independent of φ. The values of the parameters are as in Fig. 2.

modulated with the same periodicity as the lateral force (see Fig. 2).

Formation of the quasiperiodic surface patterns is clearly marked in the 2D map for the lateral force along the scratch as a function of the scan number n, presented in Fig. 2(c), where darker colors correspond to higher force amplitudes. The development of ripples can be seen by observing the change in the standard deviation of the lateral force with n. It shows an abrupt increase at the initial stages of wear and further growth with increase of the corrugation amplitude [Fig. 2(d)]. The mean lateral force $\langle F\rangle$ exhibits a steplike rise during the first scans and then, only gentle increase with n. The described behavior of the lateral force versus scan number has been found in the AFM experiments on KBr [11].

Figures 3(a) and 3(b) show the surface corrugations, $\langle z(x)\rangle$ and $\langle z(y)\rangle$, along and across the groove (in x and y directions), respectively, which have been found after 100 scans. The presented results have been calculated by averaging the surface height $z(x, y)$ along the y and x directions: $\langle z(x)\rangle = \frac{1}{2L_y}\int_{-L_y}^{+L_y} z(x, y)dy$ and $\langle z(y)\rangle = \frac{1}{L_x}\int_0^{L_x} z(x, y)dx$, where L_x is the scan length and L_y is a characteristic distance from the groove at which the effect of scratching is negligible. The $\langle z(x)\rangle$ profile exhibits a periodic structure with 14 mounds aligned along each side of the groove. For the chosen values of the parameters, the distance between the two adjacent mounds or pits is about 15 nm, and the distance between the two rows of mounds is about 4 nm.

Figure 3(c) displays an example of the dependence of wear [number of detached atoms, $N_{\text{det}}(n)$] on the number of scans n. The calculation shows a deviation from Archard's linear wear law [18,19], according to which a volume of the removed material should be proportional to the sliding length and normal load. Previously, AFM experiments also reported that their wear data do not fit Archard's law [3,6,7] very well, indicating that this law is not generally applicable to nanoscale wear. It should be noted that the total number of detached atoms, $N_{\text{det}}(n)$, does not provide proper information on the overall modification of the surface caused by the wear, since some surface sites which were scratched at earlier stages of the process could be repaired (refilled by atoms) at later stages. The actual surface abrasion is given by the integral deviation of the surface from the flat one, and it can be defined as $N_{\text{abr}}(n) = \frac{1}{a^3}\int_{L_x} dx \int_{-L_y}^{L_y} dy|z(x, y)|$. Figure 3(c) shows that $N_{\text{abr}}(n)$ can be significantly smaller than $N_{\text{det}}(n)$, and it exhibits strongly nonlinear dependence on n. A deviation of $N_{\text{abr}}(n)$ from $N_{\text{det}}(n)$ grows with a decrease in the impact angle φ since for small φ, the removed atoms are deposited closer to the scan line and the "healing" effect is more pronounced. Our simulations show that for $\varphi \leq \pi/4$, the abrasion, $N_{\text{abr}}(n)$, levels off at high scan numbers, and the increase of the ripple amplitude is saturated. On the time scale of the simulations, the saturation does not occur for higher impact angles.

An important question is what parameters of the system define the periodicity of the patterns generated by mechanical action of the tip [2,7,11,12]. Our simulations show that at the crest of each ripple the tip becomes detached from the surface, and the length of the detached

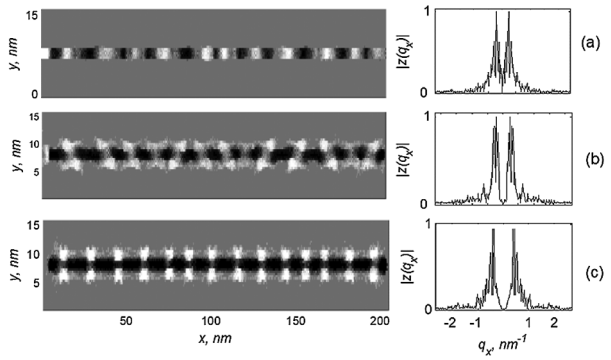

FIG. 4. Left and right columns present the gray-scale maps for the surface height $z(x, y)$ in the $\{x, y\}$ plane and the Fourier transforms $|z(q_x)|$ of the corrugation along the groove $\langle z(x)\rangle$, which have been calculated for three impact angles, $\varphi = 0$ (a), $\frac{\pi}{6}$ (b), $\frac{\pi}{4}$ (c). The maps display the mounds and pits as light and dark colors, respectively; the Fourier transforms are normalized to the maximum values of $|z(q_x)|$. The values of the parameters are as in Fig. 2.

phase of motion determines a distance between the adjacent mound and pit. This mechanism is similar to what has been found at the macroscale for unpaved roads, where the upward bounce of a wheel drives the bifurcation to the rippled state [20]. As for the nanoscale, corrugated patterns arise on roads over a wide range of material parameters, and in all cases exhibit qualitatively identical features. However, there is a significant difference in the nature of the bifurcation at the macro- and nanoscales. In the case of roads the rippled state develops only for the driving velocities which are above a critical value, and the patterns strongly depend on the velocity and mass of the wheel [20]. In the AFM configuration the detachment of the tip from the surface results from the intrinsic elastic instability of the system including the tip-substrate contact and driving spring [19,21]. The instability is velocity independent, and because of this the scan velocity does not affect the scratching process. The simulations performed in a wide range of velocities, $20\ \text{nm/s} \leq V \leq 2 \times 10^3\ \text{nm/s}$, support this conclusion [22]. At the nanoscale the instability is controlled by the tip-mound interactions that are mainly determined by the impact angle φ, tip radius (modeled by the radius of tip-surface interaction r_0), and normal load. The simulations indeed reveal that the period of the patterns increases with r_0 and with the normal load [22]. However, these effects are less pronounced than the influence of the impact angle on the topography.

Figure 4 demonstrates a pronounced effect of the impact angle (that depends on the tip geometry) on the undulated topography. The left column shows gray-scale maps for the surface height $z(x, y)$ in the $\{x, y\}$ plane, calculated for three impact angles, $\varphi = 0$, $\frac{\pi}{6}$, $\frac{\pi}{4}$. Here, mounds and pits are displayed by light and dark colors, respectively. The right column presents the Fourier transforms $|z(q_x)|$ of the corrugation along the grooves $\langle z(x)\rangle$, which exhibit well-defined maxima at the wave vectors corresponding to the periodicity of the patterns. We found that for all values of the impact angles, the scratching produces quasiperiodic patterns. The period of the patterns decreases with an increase in φ, while the spacing between the mounds and the scan line increases. Thus, our model shows that the tip geometry is the main factor influencing the topography of the grooves, as it was found in experiments [11], where the topography varied significantly between experiments using different tips.

This work, as part of the ESF EUROCORES Program FANAS (ACOF, AQUALUBE), was supported by the Israel Science Foundation (1109/09) and the Deutsche Forschungsgemeinschaft. A. F. thanks the School of Chemistry at Tel Aviv University and Institute of Mechanics at Berlin University of Technology for kind hospitality.

[1] R. W. Carpick and M. Salmeron, Chem. Rev. **97**, 1163 (1997).
[2] E. Gnecco, R. Bennewitz, and E. Meyer, Phys. Rev. Lett. **88**, 215501 (2002).
[3] W. Maw *et al.*, J. Appl. Phys. **92**, 5103 (2002).
[4] M. d'Accunto, Nanotechnology **15**, 795 (2004).
[5] B. Bhushan and K. J. Kwak, Appl. Phys. Lett. **91**, 163113 (2007).
[6] B. Gotsmann and M. A. Lantz, Phys. Rev. Lett. **101**, 125501 (2008).
[7] R. Bennewitz and J. T. Dickinson, MRS Bull. **33**, 1174 (2008).
[8] M. A. Lantz, D. Wiesmann, and B. Gotsmann, Nature Nanotech. **4**, 586 (2009).
[9] H. Bhaskaran *et al.*, Nature Nanotech. **5**, 181 (2010).
[10] O. M. Leung and M. C. Goh, Science **255**, 64 (1992).
[11] A. Socoliuc, E. Gnecco, R. Bennewitz, and E. Meyer, Phys. Rev. B **68**, 115416 (2003).
[12] B. Such, F. Krok, and M. Szymonski, Appl. Surf. Sci. **254**, 5431 (2008).
[13] J. Erlebacher *et al.*, Phys. Rev. Lett. **82**, 2330 (1999).
[14] R. Friedrich *et al.*, Phys. Rev. Lett. **85**, 4884 (2000).
[15] S. Kopta and M. Salmeron, J. Chem. Phys. **113**, 8249 (2000).
[16] G. I. Bell, Science **200**, 618 (1978).
[17] A. E. Filippov, J. Klafter, and M. Urbakh, Phys. Rev. Lett. **92**, 135503 (2004).
[18] J. F. Archard, J. Appl. Phys. **24**, 981 (1953).
[19] V. L. Popov, *Contact Mechanics and Friction* (Springer, New York, 2010).
[20] N. Taberlet, S. W. Morris, and J. N. McElwaine, Phys. Rev. Lett. **99**, 068003 (2007).
[21] M. H. Müser, M. Urbakh, and M. O. Robbins, Adv. Chem. Phys. **126**, 187 (2003).
[22] See supplemental material at http://link.aps.org/supplemental/10.1103/PhysRevLett.106.025502 for the effects of tipradius, load, and velocity on pattern formation.